Complex Scalar Singlet Model Benchmarks for Snowmass

Shekhar Adhikari,[1,2,∗] Samuel D. Lane,[1,†] Ian M. Lewis,[1,‡] and Matthew Sullivan[1,3,§]

[1]*Department of Physics and Astronomy, University of Kansas, Lawrence, Kansas, 66045 U.S.A.*

[2]*Department of Radiation Oncology and Molecular Radiation Sciences,*
School of Medicine, Johns Hopkins University, Baltimore, Maryland 21231

[3]*High Energy Theory Group, Physics Department,*
Brookhaven National Laboratory, Upton, New York, 11973 U.S.A.

Executive Summary: In this contribution to Snowmass 2021, we present benchmark parameters for the general complex scalar singlet model. The complex scalar singlet extension has three massive scalar states with interesting decay chains which will depend on the exact mass hierarchy of the system. We find maximum branching ratios for resonant double Standard Model-like Higgs production, resonant production of a Standard Model-like Higgs and a new scalar, and double resonant new scalar production. These branching ratios are between 0.7 and 1. This is particularly interesting because instead of direct production, the main production of a new scalar resonance may be from the *s*-channel production and decay of another scalar resonance. That is, it is still possible for discovery of new scalar resonances to be from the cascade of one resonance to another. We choose our benchmark points to have to have a large range of signatures: multi-*b* production, multi-*W* and *Z* production, and multi-125 GeV SM-like Higgs production. These benchmark points can provide various spectacular signatures that are consistent with current experimental and theoretical bounds. This is a summary of results in Ref. [1].

I. INTRODUCTION

As the search for new physics continues, the high luminosity Large Hadron Collider (HL-LHC) could very well provide the first evidence of beyond the Standard Model (BSM) physics. One of the simplest BSM scenarios is the addition of new real or complex scalar states that are singlets under the Standard Model (SM) gauge group. These complex scalar singlets also appear in more complete models [2, 3], and can help in solving fundamental questions in the field such as being dark matter candidates [4–6]. These simple singlet extensions have been extensively studied under

───────────
∗Electronic address: sadhika8@jhmi.edu
†Electronic address: samuel.lane@ku.edu
‡Electronic address: ian.lewis@ku.edu
§Electronic address: msullivan1@bnl.gov

the assumption they have some additional softly broken symmetries such as a $U(1)$ or $\mathbb{Z}_2$ [6, 7]. Complex scalar singlet extensions are particularly interesting because there are two scalar states in addition to the Higgs boson. Indeed, it could be that both new resonances could be discovered by one decaying into the other.

In this paper we summarize results from Ref. [1]. We consider the general complex scalar singlet extension of the SM with no additional symmetries [8]. This model extends the SM by two new CP even scalars. We find benchmark points that maximize the various di-scalar resonant productions at the HL-LHC: double 125 GeV SM-like Higgs bosons, SM-like Higgs in association with a new scalar, and two heavy new scalar bosons. This model is equivalent to the SM extended by adding two real scalar singlet extension with no additional symmetries beyond the SM. Benchmarks for two real singlet extensions with Z_2 symmetries have been studied previously [9, 10]. In section II, we introduce the model and discuss the phenomenology of the scalar sector. In section III we explore the current constraints on the model and in section IV present various benchmark points of phenomenological interest for the High Luminosity upgrade at the Large Hadron Collider (HL-LHC).

II. MODEL

Following Ref. [8], we use the most general scalar potential involving the complex scalar singlet, $S_c = (S_0 + i\,A)/\sqrt{2}$, and the Higgs doublet, $\Phi = (0, (v_{EW} + h)/\sqrt{2})^{\mathrm{T}}$ in the unitary gauge. S_0, A, and h are all real CP even scalar fields, and $v_{EW} = 246$ GeV is the Higgs vacuum expectation value. The scalar potential can be written as

$$
\begin{aligned}
V(\Phi, S_c) =\ & \frac{\mu^2}{2}\Phi^\dagger\Phi + \frac{\lambda}{4}(\Phi^\dagger\Phi)^4 + \frac{b_2}{2}|S_c|^2 + \frac{d_2}{4}|S_c|^4 + \frac{\delta_2}{2}\Phi^\dagger\Phi|S_c|^2 \\
& + \left(a_1 S_c + \frac{b_1}{4}S_c^2 + \frac{e_1}{6}S_c^3 + \frac{e_2}{6}S_c|S_c|^2 + \frac{\delta_1}{4}\Phi^\dagger\Phi\,S_c + \frac{\delta_3}{4}\Phi^\dagger\Phi\,S_c^2 \right. \\
& \left. + \frac{d_1}{8}S_c^4 + \frac{d_3}{8}S_c^2|S_c|^2 + \text{h.c.} \right)
\end{aligned}
\tag{1}
$$

where $a_1, b_1, e_1, e_2, \delta_1, \delta_3, d_1, d_3$ are complex parameters. As shown in Refs. [8, 11, 12], we can set $\langle S_c \rangle = 0$ without loss of generality.

The model contains three scalar mass eigenstates, h_1, h_2 and h_3 with masses m_1, m_2, and m_3, respectively. We will take h_1 to be the discovered Higgs boson with mass $m_1 = 125$ GeV. The mass eigenstates can be obtained from the gauge states via a $SO(3)$ rotation with three rotation angles, θ_1, θ_2, and θ_3. The θ_3 angle may be removed by appropriate choice of S_c phase [8]. Taking

the small mixing limit in θ_2, the mass eigenstates are given by transformation

$$\begin{pmatrix} h_1 \\ h_2 \\ h_3 \end{pmatrix} = \begin{pmatrix} \cos\theta_1 & -\sin\theta_1 & 0 \\ \sin\theta_1 & \cos\theta_1 & \sin\theta_2 \\ \sin\theta_1\sin\theta_2 & \cos\theta_1\sin\theta_2 & -1 \end{pmatrix} \begin{pmatrix} h \\ S_0 \\ A \end{pmatrix} + \mathcal{O}(\sin^2\theta_2). \tag{2}$$

The couplings of h_2 and h_3 to SM fermions and gauge bosons are inherited via the mixing with the SM-like Higgs boson. We see that h_2 will couple to SM fermions and gauge bosons with couplings suppressed by a factor of $\sin\theta_1$, regardless of the size of θ_2. Thus, we expect h_2 productions modes will be similar to that of the SM Higgs but with mass of m_2.

The coupling of h_3 to SM fermions and gauge bosons is doubly suppressed by the factor $\sin\theta_1\sin\theta_2$. Therefore, we expect the dominant production of h_3 to be from decays of h_2, when it is kinematically allowed. With this in mind, we will restrict ourselves to to the mass ordering $m_2 > m_3 > m_1$.

III.   CONSTRAINTS

The theoretical constraints we consider are narrow width, perturbative unitarity, boundedness, and global minimization. We restrict our parameters such that the total width of h_2 is less than 10% of its mass. We ensure perturbative unitarity is not violated at tree level by first computing the $J = 0$ partial wave matrix for two-to-two scalar scattering through the quartic couplings. Then we numerically diagonalize and make sure the eigenvalues are less than $1/2$. Finally we check that the numerically found global minima of the potential corresponds to the electroweak minima, $\langle\Phi\rangle = (0, v_{EW}/\sqrt{2})^{\mathrm{T}}$ and $\langle S_c\rangle = 0$, where $v_{EW} = 246$ GeV.

We now turn to the current experimental constraints on the model. Note that all SM-like rates and branching ratios are taken from the LHC Higgs Cross Section Working group suggested values [13]. First, we consider the signal strengths of Higgs precision measurements. In our model the production cross sections for h_1 are suppressed by a factor of $\cos^2\theta_1$, while the branching ratios remain unchanged. Thus we expect for each production mode i and decay chain $i \to h_1 \to f$ the signal strength is

$$\mu_i^f = \frac{\sigma_i(pp \to h_1)\mathrm{BR}(h_1 \to f)}{\sigma_{i,\mathrm{SM}}(pp \to h_1)\mathrm{BR}_{\mathrm{SM}}(h_1 \to f)} = \cos^2\theta_1, \tag{3}$$

where the subscript SM indicates SM values, and the numerator is calculated in the complex scalar singlet model. We then fit the mixing angle θ_1 using a χ^2 fit to the measured signal strengths [1].

Next, we turn our attention to the direct searches for heavy scalars [1]. We will need the production cross section and branching ratios to SM final states in order to implement these constraints. As stated in section II the couplings between h_2 and fermions and gauge bosons are suppressed by a factor of $\sin\theta_1$. Thus, the production rates and partial widths are given by

$$\sigma(pp \to h_2) \approx \sin^2\theta_1 \sigma_{\rm SM}(pp \to h_2), \quad \Gamma(h_2 \to f_{\rm SM}) \approx \sin^2\theta_1 \Gamma_{\rm SM}(h_2 \to f_{\rm SM}), \tag{4}$$

where $\sigma_{\rm SM}$ and $\Gamma_{\rm SM}$ indicate SM Higgs rates at the mass m_2 and $f_{\rm SM}$ are SM gauge bosons and fermions. We also consider the decay widths for $h_2 \to h_1 h_1$, $h_1 h_3$, or $h_3 h_3$, when the masses place us in the kinematically allowed region.

Normally, a "hard cut" is imposed to determine such constraints. Parameter points are rejected if their predicted cross sections are greater than any observed limit. However, this does not allow for large fluctuations for individual channels with small fluctuations in other channels. On the other hand if we use our method detailed in [14], we construct a channel-by-channel χ^2 for the heavy resonant searches to consistently combine all heavy scalar search channels and the Higgs signal strength measurements. In this method the χ^2 squared function for each channel is

$$\left(\chi^f_{i,h_2}\right)^2 = \begin{cases} \left(\dfrac{\sigma_i(pp \to h_2)\mathrm{BR}(h_2 \to f) + \hat{\sigma}^f_{i,Exp} - \hat{\sigma}^f_{i,Obs}}{\hat{\sigma}^f_{i,Exp}/1.96}\right)^2 & \text{if } \hat{\sigma}^f_{i,Obs} \geq \hat{\sigma}^f_{i,Exp} \\[4mm] \left(\dfrac{\sigma_i(pp \to h_2)\mathrm{BR}(h_2 \to f)}{\hat{\sigma}^f_{i,Obs}/1.96}\right)^2 & \text{if } \hat{\sigma}^f_{i,Obs} < \hat{\sigma}^f_{i,Exp}. \end{cases} \tag{5}$$

where $\sigma_i(pp \to h_2)$ is the resonance production cross section from initial state i, $\mathrm{BR}(h_2 \to f)$ is the branching ratio into final state f, $\hat{\sigma}^f_{i,Exp}$ ($\hat{\sigma}^f_{i,Obs}$) is the experimentally determined expected (observed) 95% CL upper limit on $\sigma(i \to h_2)\mathrm{BR}(h_2 \to f)$. For a single channel, this reproduces the traditional "hard cut" method, but allows us to combine multiple channels into a global $\Delta\chi^2$.

In Figure 1(a) we compare the resulting 95% confidence level constraints on $|\sin\theta_1|$ vs m_2 using a Higgs signal strength fit (solid black), heavy scalar searches using a traditional hard cut (dashed red), heavy scalar searches fitting a combined $\Delta\chi^2$ [Eq. (5)] across relevant channels (dot-dot-dashed magenta), and the total combined $\Delta\chi^2$ for heavy scalar searches and Higgs fits (solid blue). We have taken $\mathrm{BR}(h_2 \to h_3 X) = 0$ for $X = h_1$ or h_3. This will correspond to the most constraining case since this will force h_2 to decay to only SM final states. Here we see that for the heavy scalar searches that the $\Delta\chi^2$ are consistently stronger than the traditional hard cut. However, for $m_2 \gtrsim 650$ GeV, Higgs signal strengths are stronger than the hard cuts. Hence, in the usual method the Higgs signal strength bound $|\sin\theta_1| \lesssim 0.2$ would be used. However, for $m_2 \gtrsim 800$ GeV, the combined $\Delta\chi^2$ is less constraining than the Higgs signal strength fits since our
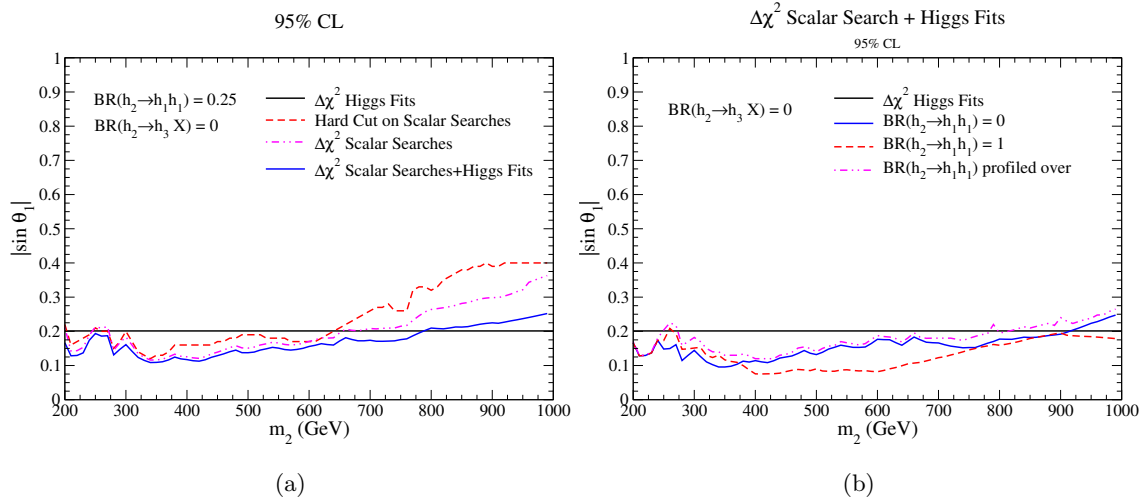
FIG. 1: In both (a) and (b) black solid lines show $\Delta\chi^2$ fits to Higgs signal strength data. (a) Bounds on $\sin\theta_1$ with BR($h_2 \to h_1 h_1$)=0.25 for (red dashed) "hard cuts" on scalar resonance searches, (magenta dot-dot-dashed) $\Delta\chi^2$ fit to scalar resonance searches, and (blue solid) combined $\Delta\chi^2$ fits to Higgs precision and resonant scalar searches. (b) Comparison of combined $\Delta\chi^2$ fits to Higgs precision data and resonant scalar searches for (blue solid) BR($h_2 \to h_1 h_1$) = 0, (red dashed) BR($h_2 \to h_1 h_1$) = 1, and (magenta dot-dot-dashed) profiling over BR($h_2 \to h_1 h_1$). In both (a,b) BR($h_2 \to h_1 h_3$) = BR($h_2 \to h_3 h_3$) = 0.

method allows for more fluctuation.

In Figure 1(b), we show the comparison of 95% confidence level constraints on $|\sin\theta_1|$ vs m_2 using the $\Delta\chi^2$ method for Higgs Fits (solid black) and Higgs signal strength fits + direct scalar searches for BR($h_2 \to h_1 h_1$) = 0, 1, and profiled (respectively solid blue, dashed red, and dot-dot-dashed magenta). We see that profiling BR($h_2 \to h_1 h_1$) is the least constraining, while the most constraining alternates between BR($h_2 \to h_1 h_1$) = 0 and 1. We will take the most constraining $\sin\theta_1$ from this plot for our benchmark points.

IV. BENCHMARK POINTS

Our benchmarks are created by maximizing resonant di-scalar production while keeping the total width of h_2 less than 10% of m_2. In practice, for current $\sin\theta_1$ bounds, this means maximizing the branching ratios of a resonant scalar h_2 into double SM-like Higgs bosons $h_2 \to h_1 h_1$, a SM-like Higgs boson and new scalar $h_2 \to h_1 h_3$, and two new scalars $h_2 \to h_3 h_3$. The maximum BR($h_2 \to h_1 h_3$) and BR($h_2 \to h_3 h_3$) will be large enough to effectively nullify direct heavy scalar search bounds. Hence, for $h_2 \to h_1 h_3$ and $h_2 \to h_3 h_3$ we only consider $\sin\theta_1$ constraints from

(a)

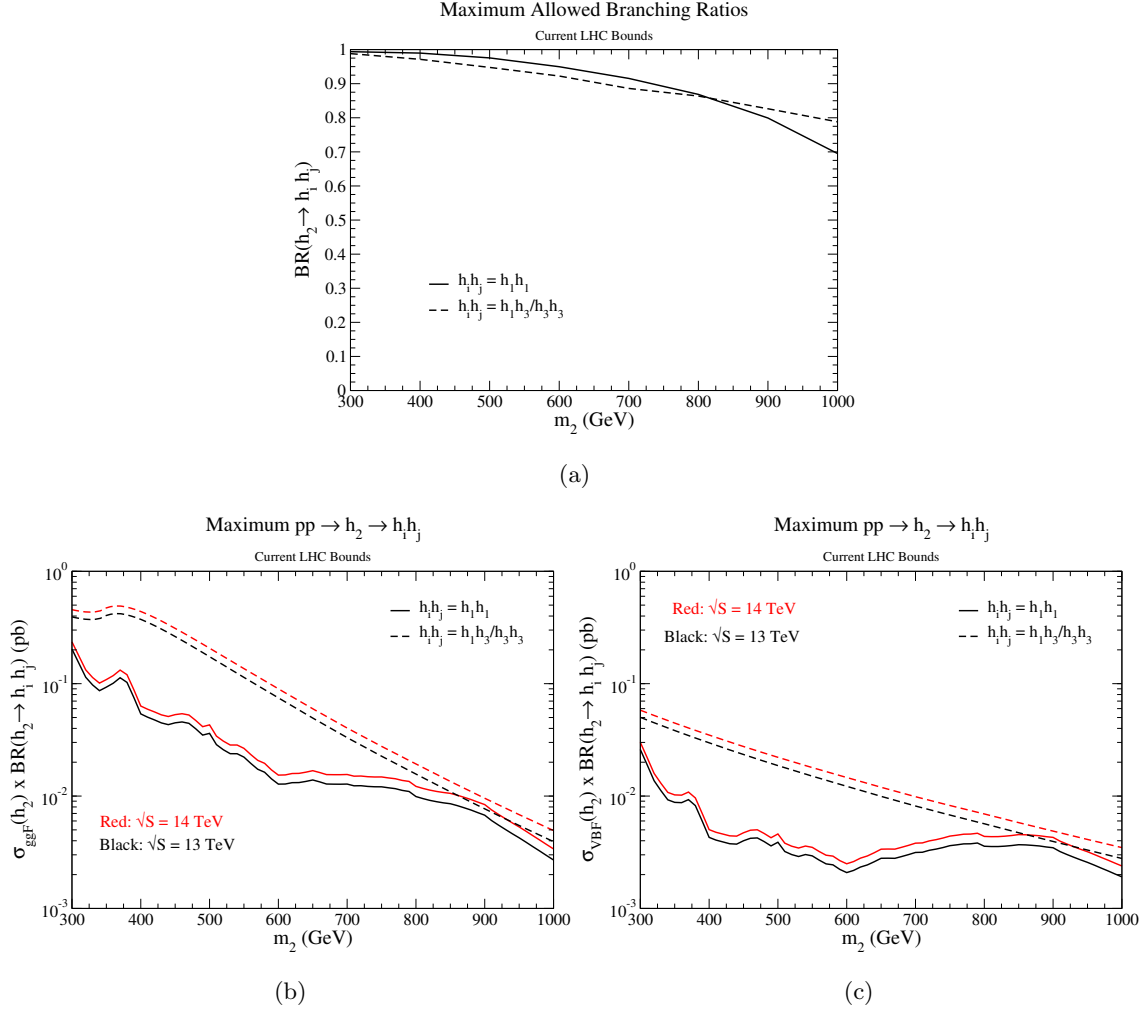(b)   (c)

FIG. 2: (a) Maximum allowed branching ratios with current LHC data for (solid) $h_1 h_1$ resonance and (dashed) $h_1 h_3$ and $h_3 h_3$ resonance. (c,d) Maximum h_2 production and decay rates for (solid) $h_2 \to h_1 h_1$ and (dashed) $h_2 \to h_1 h_3/h_3 h_3$. Red lines are for a 14 TeV LHC and black for a 13 TeV LHC. Both (c) gluon fusion and (d) vector boson fusion production rates are shown. It is required that $\Gamma_{\mathrm{Tot}}(h_2) \leq 0.1\, m_2$.

precision Higgs signal strength measurements and set $\sin\theta_1 = 0.201$. For $h_2 \to h_1 h_1$ direct scalar searches are relevant. Hence, conservatively, we set $\sin\theta_1$ to be the minimum of all constraints in Fig. 1(b).

The results are shown in Fig. 2 for (a) maximum branching ratios, (b) maximum h_2 production and decay rates in the gluon fusion channel, and (c) maximum h_2 production and decay rates in the vector boson fusion channel. Some comments are in order:

- The maximum branching ratios of $h_2 \to h_1 h_3$ and $h_2 \to h_3 h_3$ are the same. Additionally, while kinematically allowed, the maximum branching ratios are independent of the mass of

h_3. (We have checked this for $m_3 = 130$, 200, and 270 GeV, as shown in Tabs. II III). This can be understood by noting that for a given total width $\Gamma_{\text{Tot}}(h_2)$, h_2 branching ratios have an upper limit

$$\text{BR}(h_2 \to h_i h_j) \leq 1 - \frac{\sin^2 \theta_1 \Gamma_{\text{SM}}(h_2)}{\Gamma_{\text{Tot}(h_2)}}, \tag{6}$$

where $\Gamma_{\text{SM}}(h_2)$ is the total width of a SM-like Higgs with mass m_2. There is enough freedom in this model such that maximum branching ratios for $h_2 \to h_1 h_3$ and $h_2 \to h_3 h_3$ in Fig. 2(a) saturate this bound for $\Gamma_{\text{Tot}}(h_2) = 0.1 \, m_2$.

- The maximum $h_2 \to h_1 h_1$ is different than $h_2 \to h_1 h_3$ and $h_2 \to h_3 h_3$. First, this is because the $\sin \theta_1$ used is different. As we showed in Ref. [12], for smaller mixing angles we can get large branching ratios. Although, as shown in Fig. 2(b,c) the rates are smaller.

  The other effect is that $h_2 \to h_1 h_1$ does not always saturate the maximum in Eq. (6). In the small angle limit, the relevant scalar trilinear couplings are

$$
\begin{aligned}
h_1 h_1 h_2 \; &: \; \sin \theta_1 \frac{m_2^2 + 2\, m_1^2 - [\text{Re}(\delta_3) + \delta_2]\, v^2}{v} + \mathcal{O}(\sin^2 \theta_1), \\
h_1 h_2 h_3 \; &: \; \frac{\text{Im}(\delta_3)}{2} v + \mathcal{O}(\sin \theta_1), \\
h_2 h_3 h_3 \; &: \; -\frac{1}{\sqrt{2}} \left(\text{Re}(e_1) - \frac{1}{3}\text{Re}(e_2) \right) + \mathcal{O}(\sin \theta_1).
\end{aligned}
\tag{7}
$$

  The $h_2 - h_1 - h_1$ coupling has the same $\sin \theta_1$ suppression as the couplings of h_2 to SM gauge bosons and fermions. Hence, for $h_2 \to h_1 h_1$ to saturate the maximum branching ratio bound, the quartics $\text{Re}(\delta_3)$ and δ_2 have to be very large. However, perturbative unitarity bounds place strong constraints on this couplings.

In Tables I, II, and III we give the maximum branching ratios and production rates for $h_2 \to h_1 h_1$, $h_2 \to h_1 h_3$, and $h_2 \to h_3 h_3$, respectively, as well as the parameter points that generate these branching ratios and rates. We choose the mass points $m_2 = 400, 600,$ and 800 GeV, and $m_3 = 130$, 200, and 270 GeV. The Lagrangian parameter values in these tables are not unique. There are many possible choices that will generate the same maximum branching ratios.

When $|\sin \theta_1| \gg |\sin \theta_2| \neq 0$, our approximations above is good, and h_3 can still decay. If the mass of h_3 is below the $h_1 h_1$ threshold, h_3 will decay like a SM Higgs with mass m_3. We chose the mass points $m_3 = 130$, 200, and 270 GeV so that h_3 has different decay patterns:

- For $m_3 = 130$ the dominant decays are $h_3 \to bb$ and $h_3 \to WW$. Hence, for $h_2 \to h_1 h_3$ and $h_2 \to h_3 h_3$ the dominant final states are multi-b and multi-W.

- For $m_3 = 200$ GeV, both the WW and ZZ thresholds open up, and by far the most dominant decay channels are WW and ZZ. In this case, the dominate final states for $h_2 \to h_1 h_3$ are $bbWW$ and $bbZZ$. For $h_2 \to h_3 h_3$ the dominant final states are $4W$, $4Z$, and $WWZZ$.

- For $m_3 = 270$ GeV, the $h_3 \to h_1 h_1$ channel opens up. In the small mixing limit, the relevant trilinear is

$$h_1 h_1 h_3 : -\text{Im}(\delta_3)\, v\, \sin\theta_1 + \mathcal{O}(\sin^2\theta_1, \sin\theta_2) \tag{8}$$

hence, the branching ratio of $h_3 \to h_1 h_1$ can be substantial. Hence, it is possible to have a dominant signature be cascade Higgs decays: $h_2 \to h_1 h_3 \to 3\, h_1$ and $h_2 \to h_3 h_3 \to 4\, h_1$.

V. CONCLUSION

Extended scalar sectors are a feature of many models. Scalar singlets are a simple, but phenomenologically interesting, way to extend the Standard Model. The complex singlet extension, in particular, allows for resonant production of multiple different two scalar final states. In this work, we found benchmarks for resonant production and decays $pp \to h_2 \to h_1 h_1$, $pp \to h_2 \to h_1 h_3$, and $pp \to h_2 \to h_1 h_3$ in the complex singlet model.

For a variety of masses, we consistently find that the branching ratios for $h_2 \to h_i h_j$ can consistently be around $0.7 - 1$. This demonstrates the importance of double Higgs searches, particularly those where the final state "Higgs bosons" could be scalars other than the Standard Model-like Higgs boson. The typical "Higgs-like" decays of scalars to Standard Model fermion and gauge boson final states for h_2 are subdominant for these benchmarks. Additionally, the decays of h_2 is the main production mode of h_3 in the limit of small mixing, since all the couplings of h_3 to Standard Model fermions and gauge bosons are double mixing angle suppressed. For the complex singlet benchmarks we have presented, these generalized double Higgs channels are the essential discovery channels.

---

[1] S. Adhikari, S. D. Lane, I. M. Lewis, and M. Sullivan, "Di-Scalar Benchmarks in the Complex Singlet Model," to appear.

[2] M. Mühlleitner, M. O. P. Sampaio, R. Santos, and J. Wittbrodt, "Phenomenological Comparison of Models with Extended Higgs Sectors," *JHEP* **08** (2017) 132, arXiv:1703.07750 [hep-ph].

[3] H. Abouabid, A. Arhrib, D. Azevedo, J. E. Falaki, P. M. Ferreira, M. Mühlleitner, and R. Santos, "Benchmarking Di-Higgs Production in Various Extended Higgs Sector Models," arXiv:2112.12515 [hep-ph].

[4] M. Gonderinger, H. Lim, and M. J. Ramsey-Musolf, "Complex Scalar Singlet Dark Matter: Vacuum Stability and Phenomenology," *Phys. Rev.* **D86** (2012) 043511, arXiv:1202.1316 [hep-ph].

[5] R. Coimbra, M. O. P. Sampaio, and R. Santos, "ScannerS: Constraining the phase diagram of a complex scalar singlet at the LHC," *Eur. Phys. J.* **C73** (2013) 2428, arXiv:1301.2599 [hep-ph].

[6] M. Mühlleitner, M. O. P. Sampaio, R. Santos, and J. Wittbrodt, "ScannerS: parameter scans in extended scalar sectors," *Eur. Phys. J. C* **82** no. 3, (2022) 198, arXiv:2007.02985 [hep-ph].

[7] R. Costa, M. Mühlleitner, M. O. P. Sampaio, and R. Santos, "Singlet Extensions of the Standard Model at LHC Run 2: Benchmarks and Comparison with the NMSSM," *JHEP* **06** (2016) 034, arXiv:1512.05355 [hep-ph].

[8] S. Dawson and M. Sullivan, "Enhanced di-Higgs boson production in the complex Higgs singlet model," *Phys. Rev.* **D97** no. 1, (2018) 015022, arXiv:1711.06683 [hep-ph].

[9] T. Robens, T. Stefaniak, and J. Wittbrodt, "Two-real-scalar-singlet extension of the SM: LHC phenomenology and benchmark scenarios," *Eur. Phys. J. C* **80** no. 2, (2020) 151, arXiv:1908.08554 [hep-ph].

[10] A. Papaefstathiou, T. Robens, and G. Tetlalmatzi-Xolocotzi, "Triple Higgs Boson Production at the Large Hadron Collider with Two Real Singlet Scalars," *JHEP* **05** (2021) 193, arXiv:2101.00037 [hep-ph].

[11] C.-Y. Chen, S. Dawson, and I. M. Lewis, "Exploring resonant di-Higgs boson production in the Higgs singlet model," *Phys. Rev.* **D91** no. 3, (2015) 035015, arXiv:1410.5488 [hep-ph].

[12] I. M. Lewis and M. Sullivan, "Benchmarks for Double Higgs Production in the Singlet Extended Standard Model at the LHC," *Phys. Rev.* **D96** no. 3, (2017) 035037, arXiv:1701.08774 [hep-ph].

[13] **LHC Higgs Cross Section Working Group** Collaboration, D. de Florian *et al.*, "Handbook of LHC Higgs Cross Sections: 4. Deciphering the Nature of the Higgs Sector," arXiv:1610.07922 [hep-ph].

[14] S. Adhikari, I. M. Lewis, and M. Sullivan, "Beyond the Standard Model effective field theory: The

singlet extended Standard Model," *Phys. Rev. D* **103** no. 7, (2021) 075027, `arXiv:2003.10449` `[hep-ph]`.

m_2	m_3	BRs and width	$\sigma(pp \to h_2 \to h_1 h_1)$	Parameters
400 GeV	130 GeV	BR$(h_2 \to h_1 h_1) = 0.99$ $\Gamma_{\text{Tot}}(h_2) = 0.041\, m_2$	13 TeV ggF: 54 fb 13 TeV VBF: 4.3 fb 14 TeV ggF: 63 fb 14 TeV VBF: 5.0 fb	$d_2 = 0.190,\ \delta_2 = 23.1,\ \delta_3 = 22.7 + i\,0.0000871$ $d_1 = -0.132 - i\,0.00764,\ d_3 = 0.0485 - i\,0.000618$ $e_1 = (-33.3 - i\,14.7)v,\ e_2 = (-99.6 + i\,46.5)v$ $\sin\theta_1 = 0.0756$
	200 GeV	BR$(h_2 \to h_1 h_1) = 0.99$ $\Gamma_{\text{Tot}}(h_2) = 0.046\, m_2$	13 TeV ggF: 54 fb 13 TeV VBF: 4.3 fb 14 TeV ggF: 63 fb 14 TeV VBF: 5.0 fb	$d_2 = 0.22,\ \delta_2 = 25.2,\ \delta_3 = 24.2 + i\,0.0914$ $d_1 = -0.211 - i\,0.00610,\ d_3 = -0.00157 + i\,0.0000325$ $e_1 = (-29.1 - i\,11.7)v,\ e_2 = (-92.6 + i\,36.9)v$ $\sin\theta_1 = 0.0756$
	270 GeV	BR$(h_2 \to h_1 h_1) = 0.99$ $\Gamma_{\text{Tot}}(h_2) = 0.046\, m_2$	13 TeV ggF: 54 fb 13 TeV VBF: 4.3 fb 14 TeV ggF: 63 fb 14 TeV VBF: 5.0 fb	$d_2 = 0.22,\ \delta_2 = 25.2,\ \delta_3 = 24.2 + i\,0.0914$ $d_1 = -0.211 - i\,0.00610,\ d_3 = -0.00157 + i\,0.0000325$ $e_1 = (-29.1 - i\,11.7)v,\ e_2 = (-92.6 + i\,36.9)v$ $\sin\theta_1 = 0.0756$
600 GeV	130 GeV	BR$(h_2 \to h_1 h_1) = 0.95$ $\Gamma_{\text{Tot}}(h_2) = 0.026\, m_2$	13 TeV ggF: 13 fb 13 TeV VBF: 2.1 fb 14 TeV ggF: 15 fb 14 TeV VBF: 2.5 fb	$d_2 = 0.869,\ \delta_2 = 24.2,\ \delta_3 = 23.9 + i\,0.0243$ $d_1 = -0.356 + i\,0.122,\ d_3 = -0.343 - i\,0.0415$ $e_1 = (-33.2 - i\,10.8)v,\ e_2 = (-99.4 + i\,31.9)v$ $\sin\theta_1 = 0.0819$
	200 GeV	BR$(h_2 \to h_1 h_1) = 0.95$ $\Gamma_{\text{Tot}}(h_2) = 0.026\, m_2$	13 TeV ggF: 13 fb 13 TeV VBF: 2.1 fb 14 TeV ggF: 15 fb 14 TeV VBF: 2.5 fb	$d_2 = 0.869,\ \delta_2 = 24.2,\ \delta_3 = 23.9 + i\,0.0243$ $d_1 = -0.356 + i\,0.122,\ d_3 = -0.343 - i\,0.0415$ $e_1 = (-33.2 - i\,10.8)v,\ e_2 = (-99.4 + i\,31.9)v$ $\sin\theta_1 = 0.0819$
	270 GeV	BR$(h_2 \to h_1 h_1) = 0.95$ $\Gamma_{\text{Tot}}(h_2) = 0.026\, m_2$	13 TeV ggF: 13 fb 13 TeV VBF: 2.1 fb 14 TeV ggF: 15 fb 14 TeV VBF: 2.5 fb	$d_2 = 0.869,\ \delta_2 = 24.2,\ \delta_3 = 23.9 + i\,0.0243$ $d_1 = -0.356 + i\,0.122,\ d_3 = -0.343 - i\,0.0415$ $e_1 = (-33.2 - i\,10.8)v,\ e_2 = (-99.4 + i\,31.9)v$ $\sin\theta_1 = 0.0819$
800 GeV	130 GeV	BR$(h_2 \to h_1 h_1) = 0.87$ $\Gamma_{\text{Tot}}(h_2) = 0.066\, m_2$	13 TeV ggF: 9.9 fb 13 TeV VBF: 3.6 fb 14 TeV ggF: 12 fb 14 TeV VBF: 4.4 fb	$d_2 = 0.611,\ \delta_2 = 24.6,\ \delta_3 = 23.5 + i\,0.00901$ $d_1 = -0.0806 + i\,0.368,\ d_3 = -0.128 - i\,0.0143$ $e_1 = (-33.0 + i\,28.5)v,\ e_2 = (-99.4 - i\,91.9)v$ $\sin\theta_1 = 0.159$
	200 GeV	BR$(h_2 \to h_1 h_1) = 0.87$ $\Gamma_{\text{Tot}}(h_2) = 0.066\, m_2$	13 TeV ggF: 9.9 fb 13 TeV VBF: 3.6 fb 14 TeV ggF: 12 fb 14 TeV VBF: 4.4 fb	$d_2 = 0.611,\ \delta_2 = 24.6,\ \delta_3 = 23.5 + i\,0.00901$ $d_1 = -0.0806 + i\,0.368,\ d_3 = -0.128 - i\,0.0143$ $e_1 = (-33.0 + i\,28.5)v,\ e_2 = (-99.4 - i\,91.9)v$ $\sin\theta_1 = 0.159$
	270 GeV	BR$(h_2 \to h_1 h_1) = 0.87$ $\Gamma_{\text{Tot}}(h_2) = 0.066\, m_2$	13 TeV ggF: 9.9 fb 13 TeV VBF: 3.6 fb 14 TeV ggF: 12 fb 14 TeV VBF: 4.4 fb	$d_2 = 0.611,\ \delta_2 = 24.6,\ \delta_3 = 23.5 + i\,0.00901$ $d_1 = -0.0806 + i\,0.368,\ d_3 = -0.128 - i\,0.0143$ $e_1 = (-33.0 + i\,28.5)v,\ e_2 = (-99.4 - i\,91.9)v$ $\sin\theta_1 = 0.159$

TABLE I: Benchmark points that maximize BR$(h_2 \to h_1 h_1)$ with cross sections at the LHC.

m_2	m_3	BRs and width	$\sigma(pp \to h_2 \to h_1 h_3)$	Parameters
400 GeV	130 GeV	$\mathrm{BR}(h_2 \to h_1 h_3) = 0.97$ $\Gamma_{\mathrm{Tot}}(h_2) = 0.1\,m_2$	13 TeV ggF: 370 fb 13 TeV VBF: 30 fb 14 TeV ggF: 440 fb 14 TeV VBF: 35 fb	$d_2 = 22.9$, $\delta_2 = 3.18$, $\delta_3 = -0.332 + i\,0$ $d_1 = -4.86 - i\,3.37$, $d_3 = -3.88 - i\,2.68$ $e_1 = (-0.250 - i\,61.0)v$, $e_2 = (-2.28 + i\,94.9)v$ $\sin\theta_1 = 0.201$
	200 GeV	$\mathrm{BR}(h_2 \to h_1 h_3) = 0.97$ $\Gamma_{\mathrm{Tot}}(h_2) = 0.1\,m_2$	13 TeV ggF: 370 fb 13 TeV VBF: 30 fb 14 TeV ggF: 440 fb 14 TeV VBF: 35 fb	$d_2 = 18.5$, $\delta_2 = 1.25$, $\delta_3 = -0.0573 + i\,0$ $d_1 = -5.71 - i\,2.78$, $d_3 = -7.49 - i\,8.61$ $e_1 = (7.65 + i\,39.5)v$, $e_2 = (-21.4 - i\,16.4)v$ $\sin\theta_1 = 0.201$
	270 GeV	$\mathrm{BR}(h_2 \to h_1 h_3) = 0.97$ $\Gamma_{\mathrm{Tot}}(h_2) = 0.1\,m_2$	13 TeV ggF: 370 fb 13 TeV VBF: 30 fb 14 TeV ggF: 440 fb 14 TeV VBF: 35 fb	$d_2 = 18.7$, $\delta_2 = 0.197$, $\delta_3 = -0.0000418 + i\,0.134$ $d_1 = 7.83 + i\,2.51$, $d_3 = 0.493 + i\,3.96$ $e_1 = (72.0 + i\,86.0)v$, $e_2 = (-92.5 - i\,54.7)v$ $\sin\theta_1 = 0.201$
600 GeV	130 GeV	$\mathrm{BR}(h_2 \to h_1 h_3) = 0.92$ $\Gamma_{\mathrm{Tot}}(h_2) = 0.1\,m_2$	13 TeV ggF: 75 fb 13 TeV VBF: 12 fb 14 TeV ggF: 90 fb 14 TeV VBF: 15 fb	$d_2 = 18.2$, $\delta_2 = 3.41$, $\delta_3 = 0.258 + i\,0$ $d_1 = 5.97 + i\,2.24$, $d_3 = 2.38 + i\,7.29$ $e_1 = (-4.59 + i\,37.6)v$, $e_2 = (-15.1 + i\,6.20)v$ $\sin\theta_1 = 0.201$
	200 GeV	$\mathrm{BR}(h_2 \to h_1 h_3) = 0.92$ $\Gamma_{\mathrm{Tot}}(h_2) = 0.1\,m_2$	13 TeV ggF: 75 fb 13 TeV VBF: 12 fb 14 TeV ggF: 90 fb 14 TeV VBF: 15 fb	$d_2 = 20.8$, $\delta_2 = 1.72$, $\delta_3 = 0.503 + i\,0$ $d_1 = 6.25 + i\,1.80$, $d_3 = -4.63 + i\,6.12$ $e_1 = (-7.24 + i\,59.1)v$, $e_2 = (-22.2 - i\,53.3)v$ $\sin\theta_1 = 0.201$
	270 GeV	$\mathrm{BR}(h_2 \to h_1 h_3) = 0.92$ $\Gamma_{\mathrm{Tot}}(h_2) = 0.1\,m_2$	13 TeV ggF: 75 fb 13 TeV VBF: 12 fb 14 TeV ggF: 90 fb 14 TeV VBF: 15 fb	$d_2 = 17.9$, $\delta_2 = 0.467$, $\delta_3 = -0.0976 + i\,0.0946$ $d_1 = 4.16 - i\,2.35$, $d_3 = 3.27 - i\,3.49$ $e_1 = (-11.8 + i\,57.7)v$, $e_2 = (-35.7 - i\,39.9)v$ $\sin\theta_1 = 0.201$
800 GeV	130 GeV	$\mathrm{BR}(h_2 \to h_1 h_3) = 0.86$ $\Gamma_{\mathrm{Tot}}(h_2) = 0.1\,m_2$	13 TeV ggF: 16 fb 13 TeV VBF: 5.7 fb 14 TeV ggF: 19 fb 14 TeV VBF: 6.9 fb	$d_2 = 19.9$, $\delta_2 = 3.22$, $\delta_3 = 2.98 + i\,0$ $d_1 = 6.44 - i\,0.319$, $d_3 = 3.90 - i\,1.23$ $e_1 = (-8.89 - i\,61.0)v$, $e_2 = (-26.8 + i\,33.1)v$ $\sin\theta_1 = 0.201$
	200 GeV	$\mathrm{BR}(h_2 \to h_1 h_3) = 0.86$ $\Gamma_{\mathrm{Tot}}(h_2) = 0.1\,m_2$	13 TeV ggF: 16 fb 13 TeV VBF: 5.7 fb 14 TeV ggF: 19 fb 14 TeV VBF: 6.9 fb	$d_2 = 21.1$, $\delta_2 = 4.54$, $\delta_3 = 1.76 + i\,0.605$ $d_1 = 6.74 + i\,2.11$, $d_3 = 3.07 - i\,10.1$ $e_1 = (-11.8 - i\,46.7)v$, $e_2 = (-36.8 - i\,6.65)v$ $\sin\theta_1 = 0.201$
	270 GeV	$\mathrm{BR}(h_2 \to h_1 h_3) = 0.86$ $\Gamma_{\mathrm{Tot}}(h_2) = 0.1\,m_2$	13 TeV ggF: 16 fb 13 TeV VBF: 5.7 fb 14 TeV ggF: 19 fb 14 TeV VBF: 6.9 fb	$d_2 = 18.9$, $\delta_2 = 4.20$, $\delta_3 = 2.06 - i\,0.137$ $d_1 = 6.67 + i\,2.92$, $d_3 = 4.94 - i\,10.7$ $e_1 = (-12.0 + i\,29.6)v$, $e_2 = (-37.1 + i\,67.6)v$ $\sin\theta_1 = 0.201$

TABLE II: Benchmark points that maximize $\mathrm{BR}(h_2 \to h_1 h_3)$ with cross sections at the LHC with $\sin\theta_1 = 0.201$.

m_2	m_3	BRs and width	$\sigma(pp \to h_2 \to h_3 h_3)$	Parameters
400 GeV	130 GeV	$\mathrm{BR}(h_2 \to h_3 h_3) = 0.97$ $\Gamma_{\mathrm{Tot}}(h_2) = 0.1\,m_2$	13 TeV ggF: 370 fb 13 TeV VBF: 30 fb 14 TeV ggF: 440 fb 14 TeV VBF: 35 fb	$d_2 = 18.9$, $\delta_2 = 1.77$, $\delta_3 = -0.118 + i\,0$ $d_1 = 3.14 - i\,2.14$, $d_3 = 0.434 - i\,2.62$ $e_1 = (-8.75 - i\,20.0)v$, $e_2 = (-1.84 + i\,60.0)v$ $\sin\theta_1 = 0.201$
600 GeV	130 GeV	$\mathrm{BR}(h_2 \to h_3 h_3) = 0.92$ $\Gamma_{\mathrm{Tot}}(h_2) = 0.1\,m_2$	13 TeV ggF: 75 fb 13 TeV VBF: 12 fb 14 TeV ggF: 90 fb 14 TeV VBF: 15 fb	$d_2 = 16.5$, $\delta_2 = 3.12$, $\delta_3 = 0.604 + i\,0$ $d_1 = 7.18 + i\,1.47$, $d_3 = -1.53 - i\,6.00$ $e_1 = (-13.0 - i\,18.8)v$, $e_2 = (-6.32 + i\,56.5)v$ $\sin\theta_1 = 0.201$
	200 GeV	$\mathrm{BR}(h_2 \to h_3 h_3) = 0.92$ $\Gamma_{\mathrm{Tot}}(h_2) = 0.1\,m_2$	13 TeV ggF: 75 fb 13 TeV VBF: 12 fb 14 TeV ggF: 90 fb 14 TeV VBF: 15 fb	$d_2 = 15.2$, $\delta_2 = 1.82$, $\delta_3 = 0.155 + i\,0$ $d_1 = 1.42 + i\,2.91$, $d_3 = 12.6 + i\,5.94$ $e_1 = (-16.9 + i\,13.9)v$, $e_2 = (-14.2 - i\,41.7)v$ $\sin\theta_1 = 0.201$
	270 GeV	$\mathrm{BR}(h_2 \to h_3 h_3) = 0.92$ $\Gamma_{\mathrm{Tot}}(h_2) = 0.1\,m_2$	13 TeV ggF: 75 fb 13 TeV VBF: 12 fb 14 TeV ggF: 90 fb 14 TeV VBF: 15 fb	$d_2 = 11.1$, $\delta_2 = 0.142$, $\delta_3 = -0.0342 - i\,0.00817$ $d_1 = -5.13 - i\,5.14$, $d_3 = -3.21 + i\,0.753$ $e_1 = (-26.1 - i\,12.7)v$, $e_2 = (-29.7 + i\,38.1)v$ $\sin\theta_1 = 0.201$
800 GeV	130 GeV	$\mathrm{BR}(h_2 \to h_3 h_3) = 0.86$ $\Gamma_{\mathrm{Tot}}(h_2) = 0.1\,m_2$	13 TeV ggF: 16 fb 13 TeV VBF: 5.6 fb 14 TeV ggF: 19 fb 14 TeV VBF: 6.9 fb	$d_2 = 21.1$, $\delta_2 = 2.42$, $\delta_3 = 2.42 + i\,0$ $d_1 = 3.77 - i\,8.72$, $d_3 = 2.21 + i\,5.43$ $e_1 = (-28.0 - i\,0.44)v$, $e_2 = (-41.4 + i\,2.15)v$ $\sin\theta_1 = 0.201$
	200 GeV	$\mathrm{BR}(h_2 \to h_3 h_3) = 0.86$ $\Gamma_{\mathrm{Tot}}(h_2) = 0.1\,m_2$	13 TeV ggF: 16 fb 13 TeV VBF: 5.6 fb 14 TeV ggF: 19 fb 14 TeV VBF: 6.9 fb	$d_2 = 13.8$, $\delta_2 = 0.810$, $\delta_3 = 0.810 + i\,0$ $d_1 = -10.8 + i\,1.53$, $d_3 = 1.29 - i\,5.41$ $e_1 = (-32.6 + i\,1.05)v$, $e_2 = (-53.2 - i\,8.34)v$ $\sin\theta_1 = 0.201$
	270 GeV	$\mathrm{BR}(h_2 \to h_3 h_3) = 0.86$ $\Gamma_{\mathrm{Tot}}(h_2) = 0.1\,m_2$	13 TeV ggF: 16 fb 13 TeV VBF: 5.7 fb 14 TeV ggF: 19 fb 14 TeV VBF: 6.9 fb	$d_2 = 10.6$, $\delta_2 = 0.765$, $\delta_3 = 0.695 + i\,0.145$ $d_1 = 0.695 - i\,7.63$, $d_3 = 1.74 - i\,4.77$ $e_1 = (-28.3 - i\,20.4)v$, $e_2 = (-36.7 + i\,68.7)v$ $\sin\theta_1 = 0.201$

TABLE III: Benchmark points that maximize $\mathrm{BR}(h_2 \to h_3 h_3)$ with cross sections at the LHC with $\sin\theta_1 = 0.201$.